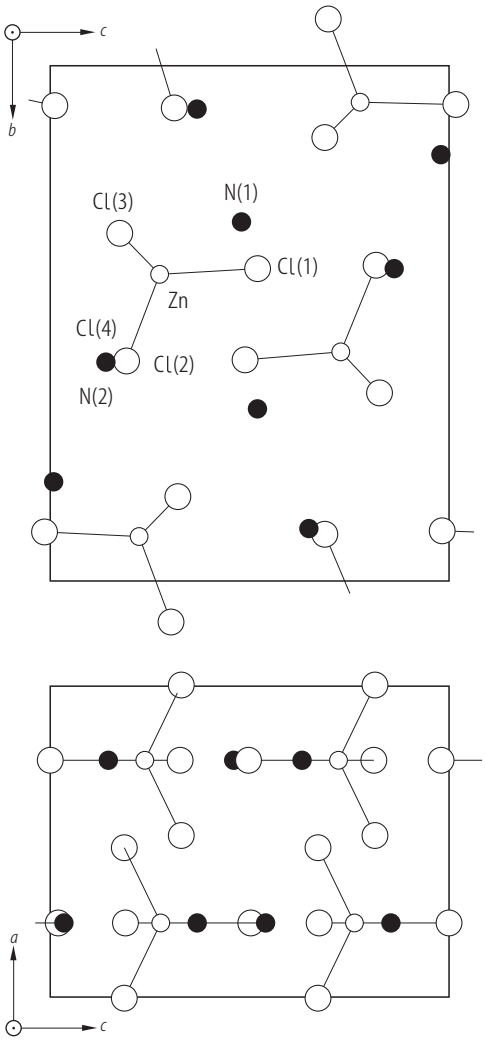

Fig. 39A-11-001. $(NH_4)_2ZnCl_4$. Structure of phase I [82Mat1]. Projections along the *a* and *b* axes. T = 418 K. Hydrogen atoms are omitted.

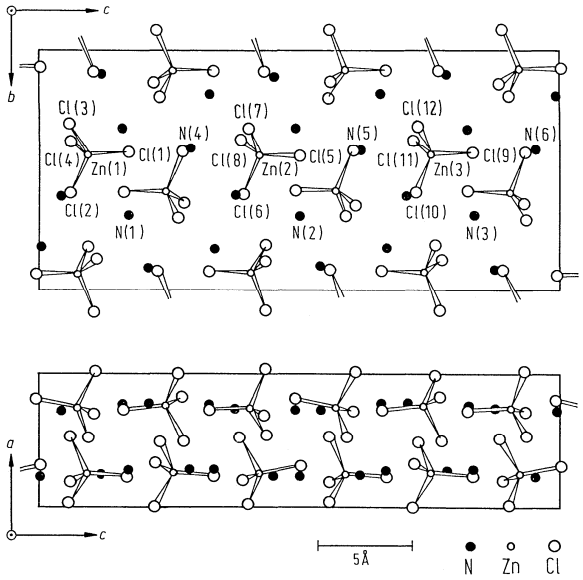

Fig. 39A-11-002. $(NH_4)_2ZnCl_4$. Structure of phase V [82Mat2]. Projections along the *a* and *b* axes. T = 223 K. Hydrogen atoms are omitted.

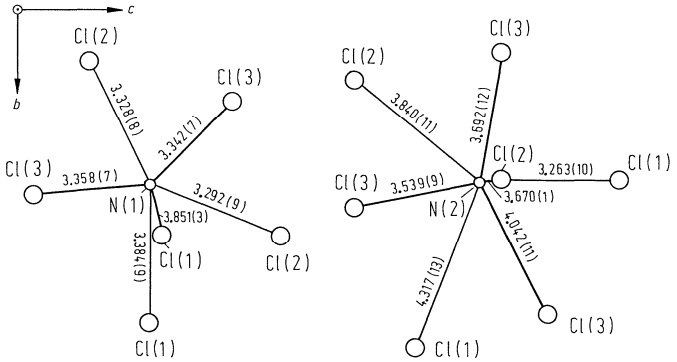

Fig. 39A-11-003. $(NH_4)_2ZnCl_4$. Structure of phase I [82Mat1]. T = 418 K. Environments of the two crystallographically independent N(1) and N(2) atoms. Views along the *a* axis. Distances in [Å].

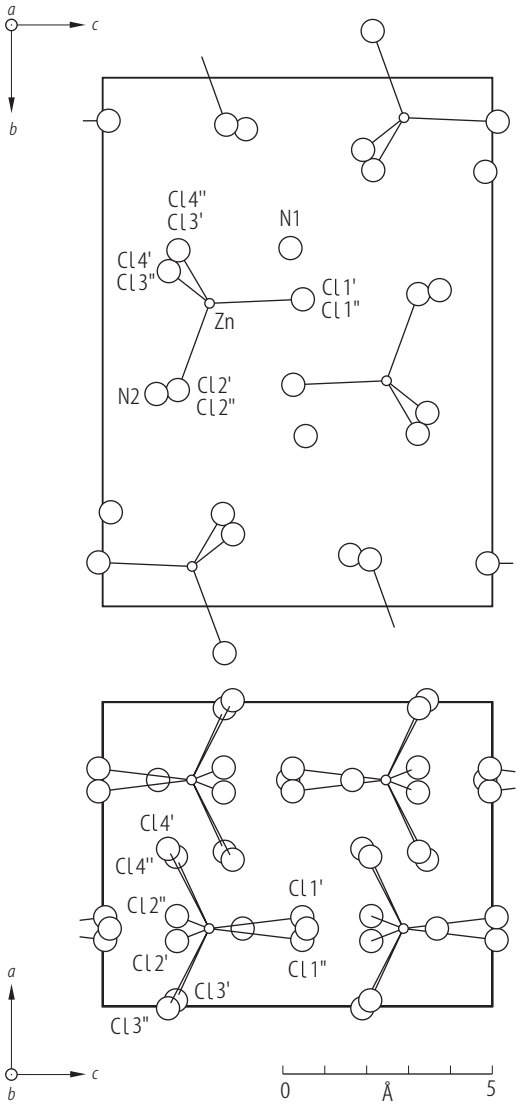

Fig. 39A-11-004. $(NH_4)_2ZnCl_4$. Structure of phase I [82Mat3]. Projections along the *a* and *b* axes. $T = 418$ K. Primed and double-primed symbols for Cl atoms represent the split atoms.

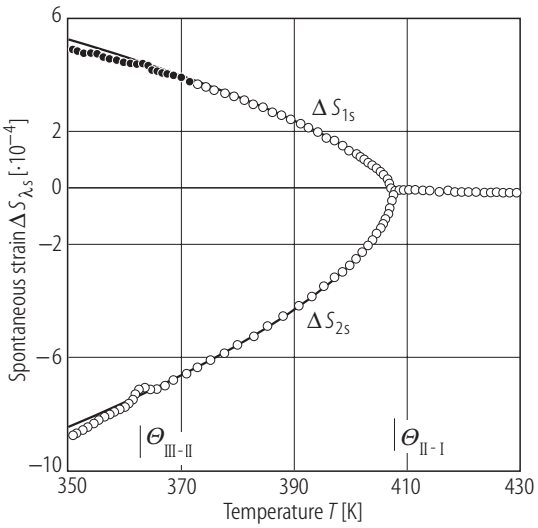

Fig. 39A-11-005. $(NH_4)_2ZnCl_4$. $\Delta S_{\lambda s}$ vs. T in phase II [90Tyl]. ΔS_{1s}, ΔS_{2s}: spontaneous strain components along the *a* and *b* axes.

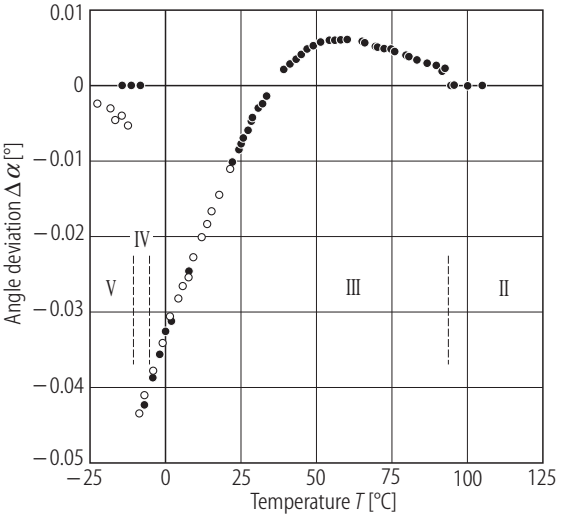

Fig. 39A-11-006. $(NH_4)_2ZnCl_4$. $\Delta\alpha$ vs. T [85Deg]. $\Delta\alpha$: deviation of axial angle α from 90°. Full circle: on heating, open circle: on cooling.

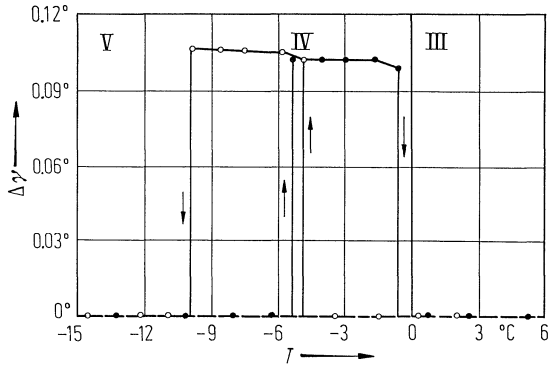

Fig. 39A-11-007. $(NH_4)_2ZnCl_4$. $\Delta\gamma$ vs. T [85Deg]. $\Delta\gamma$: deviation of axial angle γ from 90°. Full circle: on heating, open circle: on cooling.

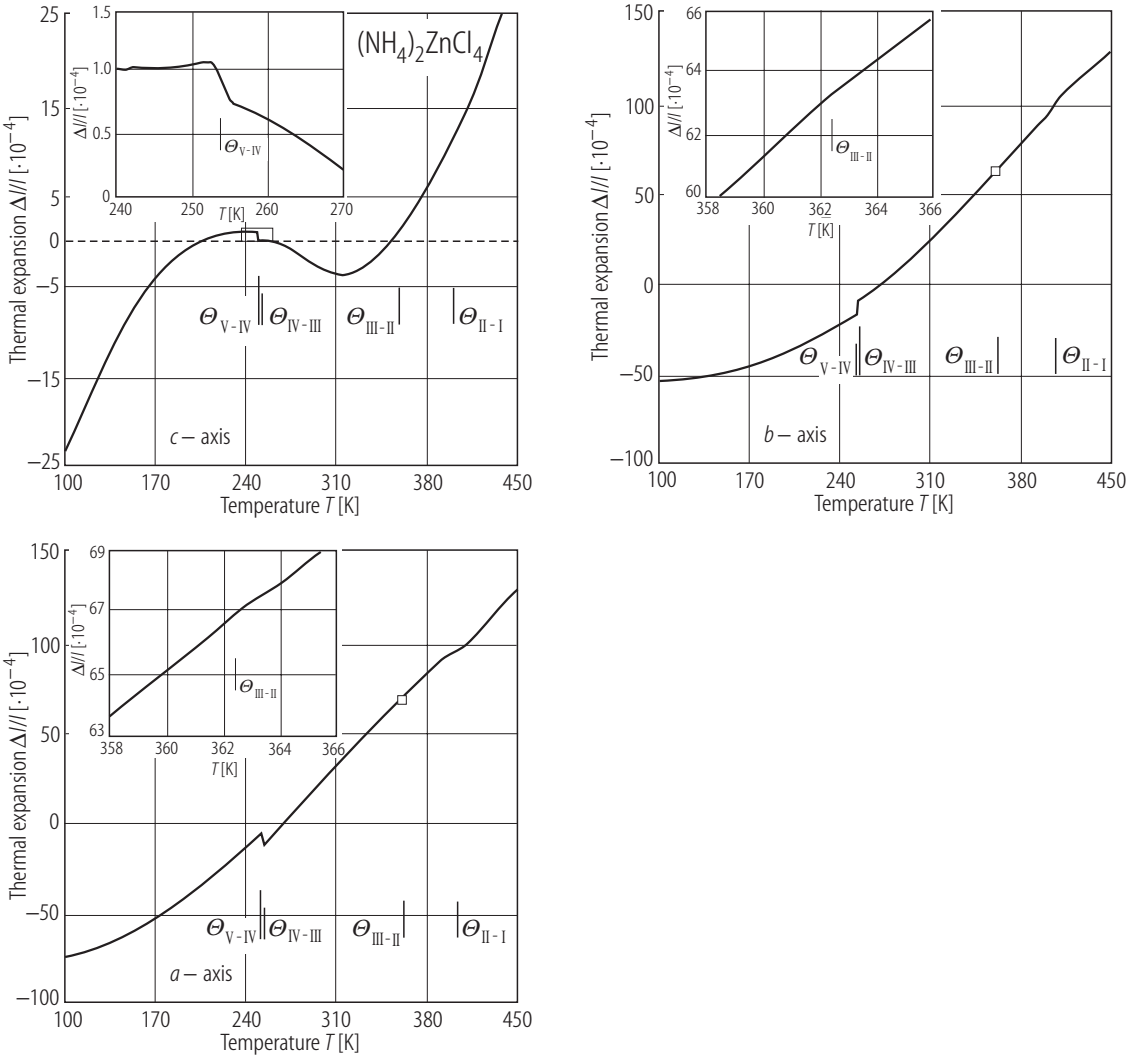

Fig. 39A-11-008. $(NH_4)_2ZnCl_4$. $\Delta l/l$ vs. T [90Tyl]. $\Delta l/l$: linear thermal expansion along the a, b and c axes.

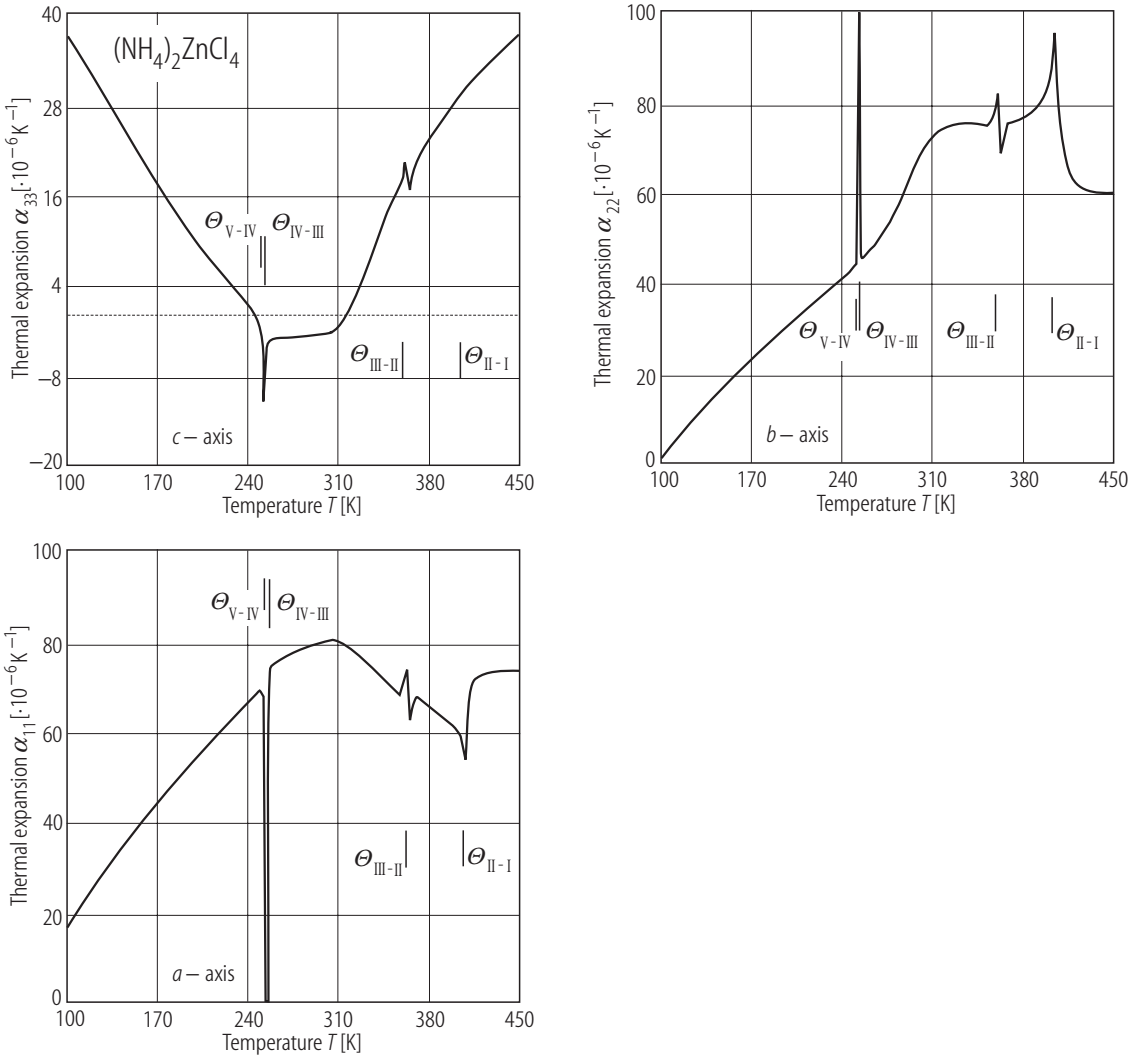

Fig. 39A-11-009. $(NH_4)_2ZnCl_4$. α_{11}, α_{22}, α_{33} vs. T [90Tyl]. α_{11}, α_{22}, α_{33}: linear thermal expansion coefficients along the *a*, *b* and *c* axes.

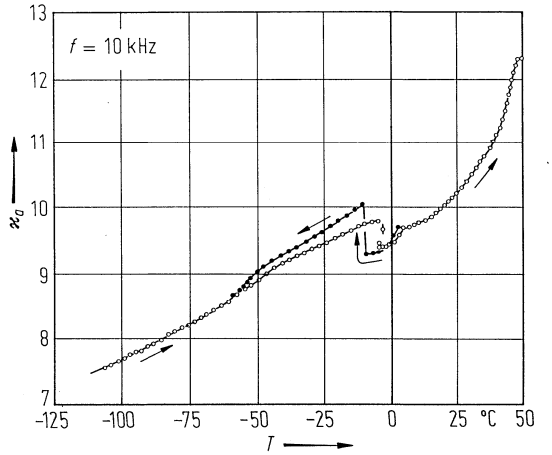

Fig. 39A-11-010. $(NH_4)_2ZnCl_4$. $\varkappa_a$ vs. T [82Sat].

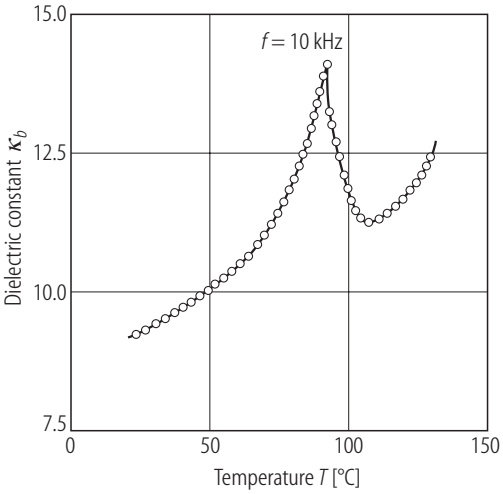

Fig. 39A-11-011. $(NH_4)_2ZnCl_4$. κ_b vs. T [84Sat]. On heating.

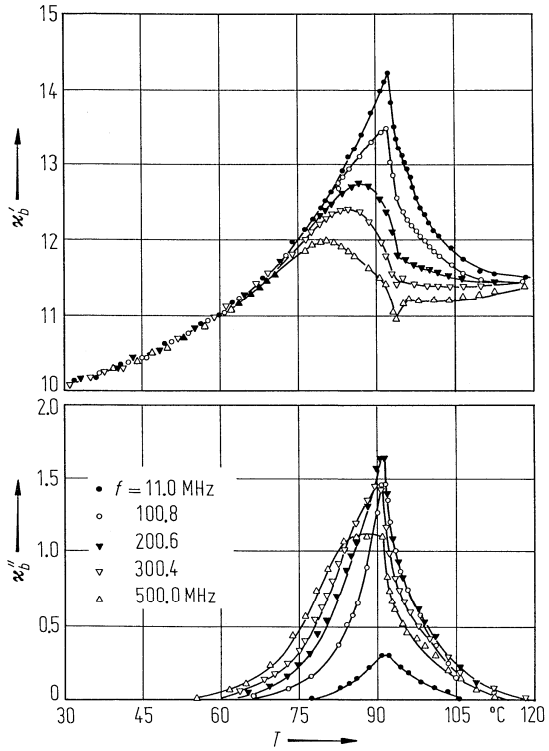

Fig. 39A-11-012. $(NH_4)_2ZnCl_4$. κ_b', κ_b'' vs. T [85Osa]. Parameter: f.

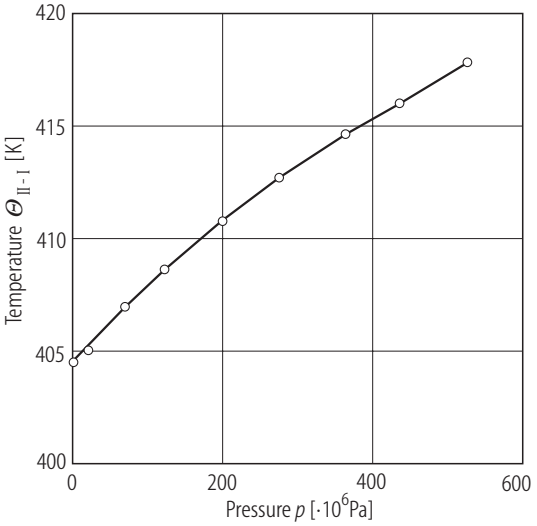

Fig. 39A-11-013. $(NH_4)_2ZnCl_4$. Θ_{II-I} vs. p [94Kit].

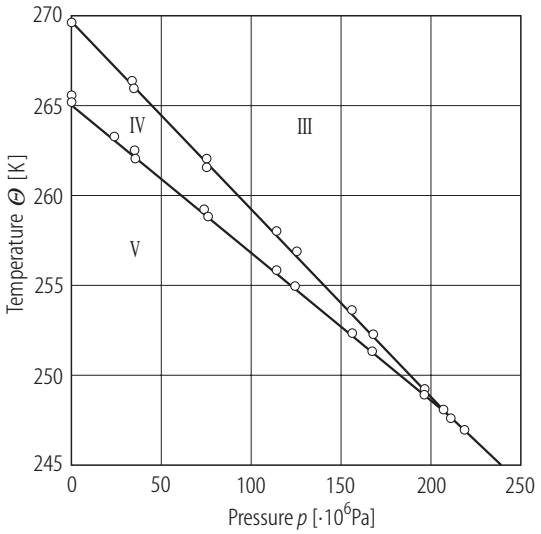

Fig. 39A-11-014. $(NH_4)_2ZnCl_4$. Θ vs. p around phase IV [94Kit].

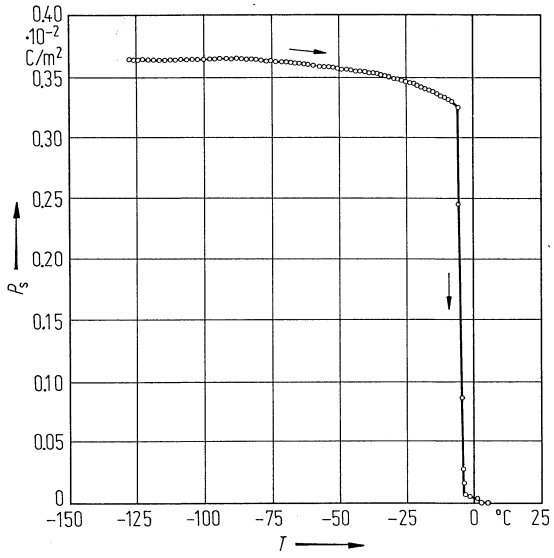

Fig. 39A-11-015. $(NH_4)_2ZnCl_4$. P_s vs. T [82Sat]. Obtained from pyroelectric charge measurements.

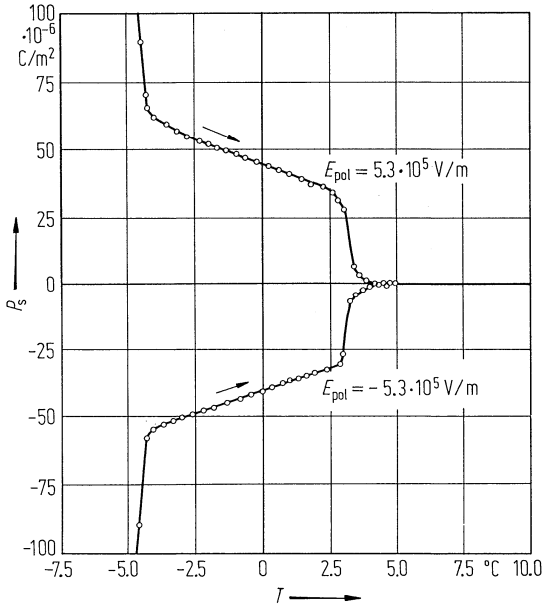

Fig. 39A-11-016. $(NH_4)_2ZnCl_4$. P_s vs. T near lower transition temperatures [82Sat]. Obtained from pyroelectric charge measurements. E_{pol}: poling field.

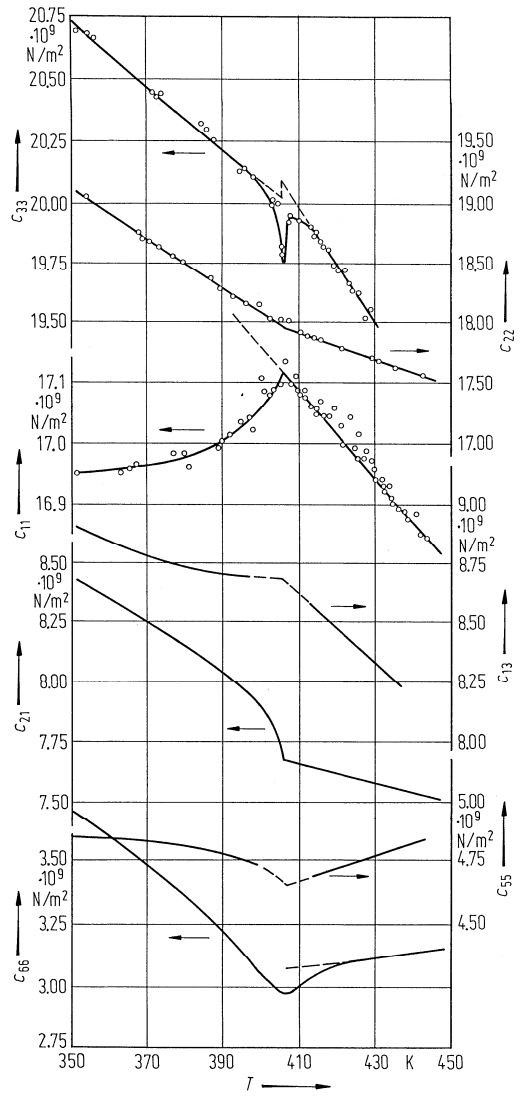

Fig. 39A-11-017. $(NH_4)_2ZnCl_4$. $c_{\lambda\mu}$ vs. T [81Smo]. Brillouin scattering. $\lambda = 514.6$ nm.

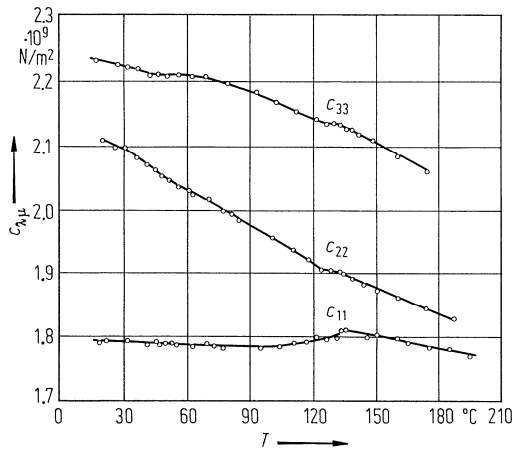

Fig. 39A-11-018. $(NH_4)_2ZnCl_4$. c_{11}, c_{22}, c_{33} vs. T [87Gil]. Brillouin scattering. $\lambda = 514.6$ nm.

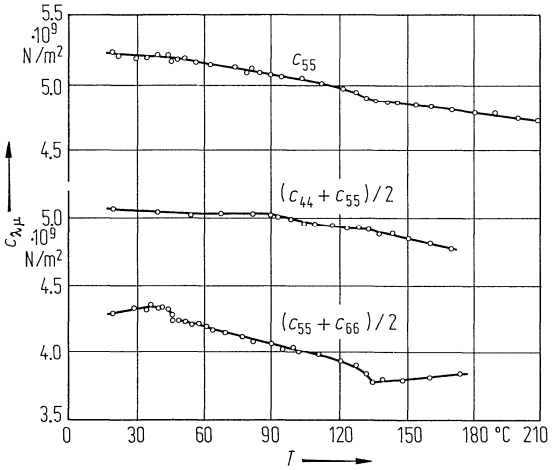

Fig. 39A-11-019. $(NH_4)_2ZnCl_4$. c_{55}, $(c_{44} + c_{55})/2$, $(c_{55} + c_{66})/2$ vs. T [87Gil]. Brillouin scattering. $\lambda = 514.6$ nm.

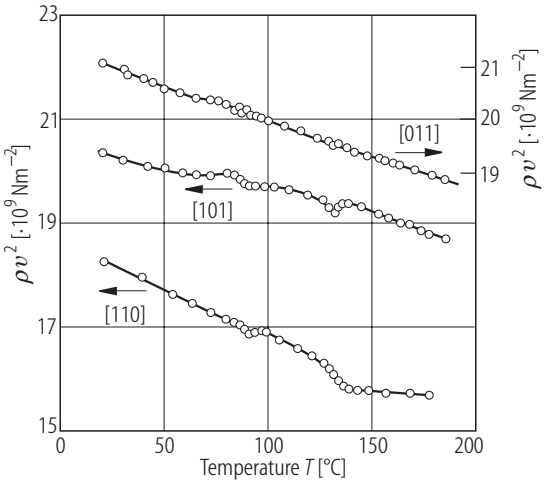

Fig. 39A-11-020. $(NH_4)_2ZnCl_4$. ρv^2 vs. T [89Lus]. v: sound velocity determined by Brillouin scattering frequency shift of the LA mode. Incident wave length: $\lambda = 514.5$ nm. Parameter: propagation direction.

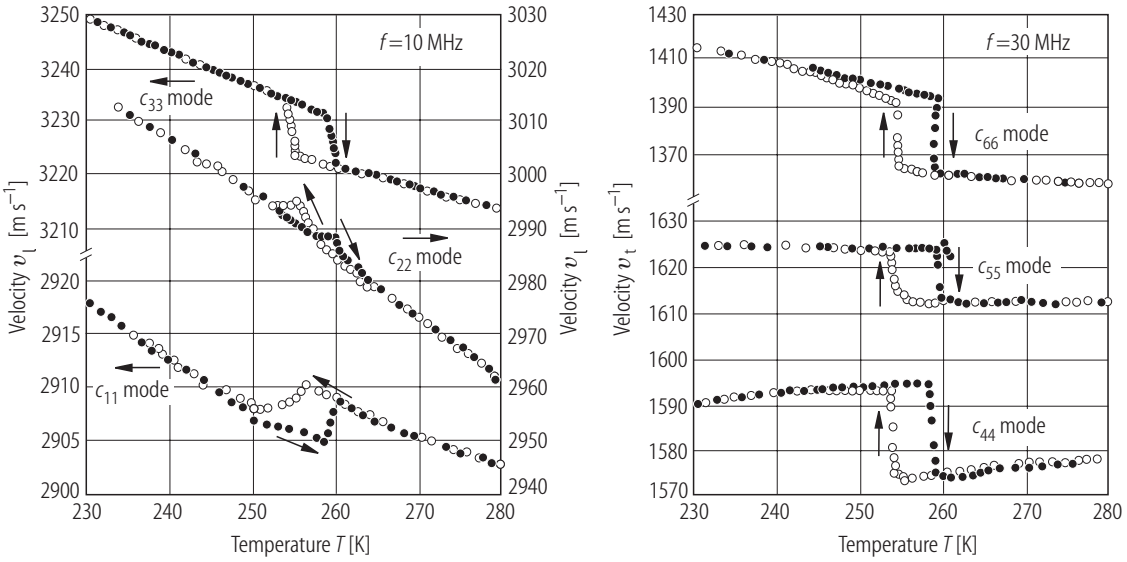

Fig. 39A-11-021. $(NH_4)_2ZnCl_4$. v_l, v_t vs. T [90Nas]. v_l, v_t: sound velocity.

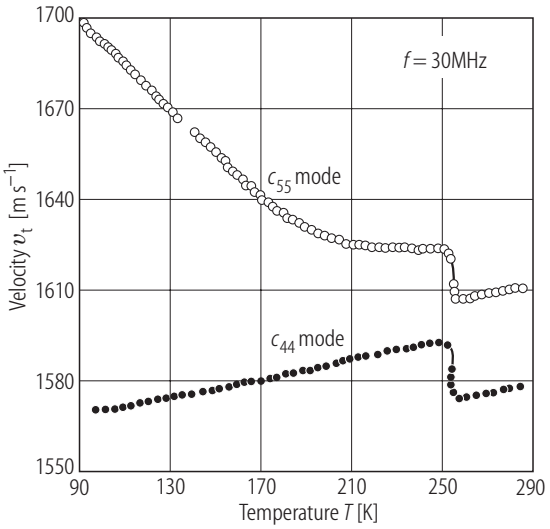

Fig. 39A-11-022. $(NH_4)_2ZnCl_4$. v_t vs. T in phase V and phase IV [90Nas]. v_t: transverse sound velocity.

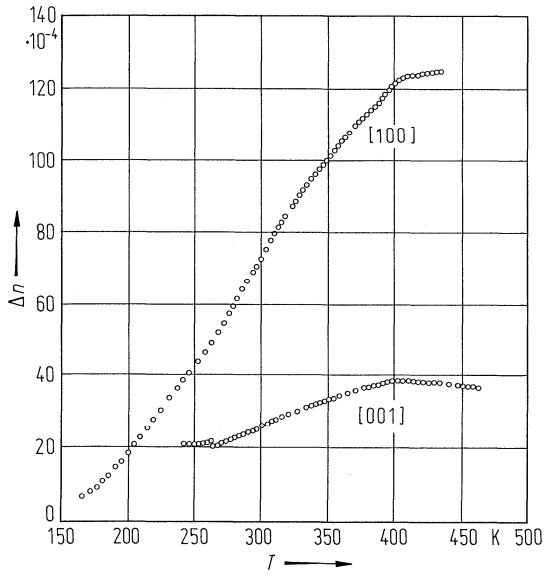

Fig. 39A-11-023. $(NH_4)_2ZnCl_4$. Δn vs. T [84Mel]. Δn: birefringence measured along [100] and [001].

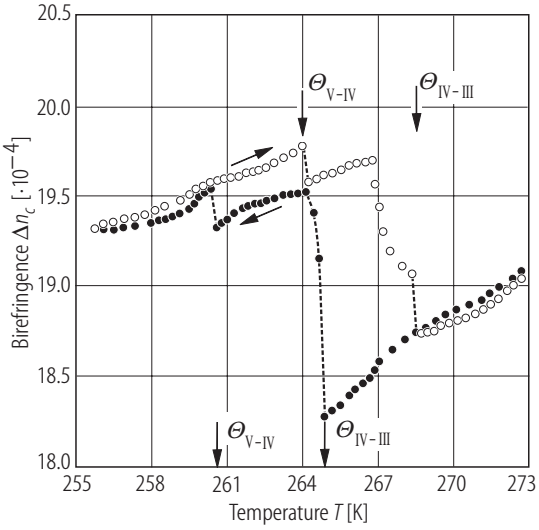

Fig. 39A-11-024. $(NH_4)_2ZnCl_4$. Δn_c vs. T near lower transition temperatures [84Mel]. Δn_c: birefringence measured along [001].

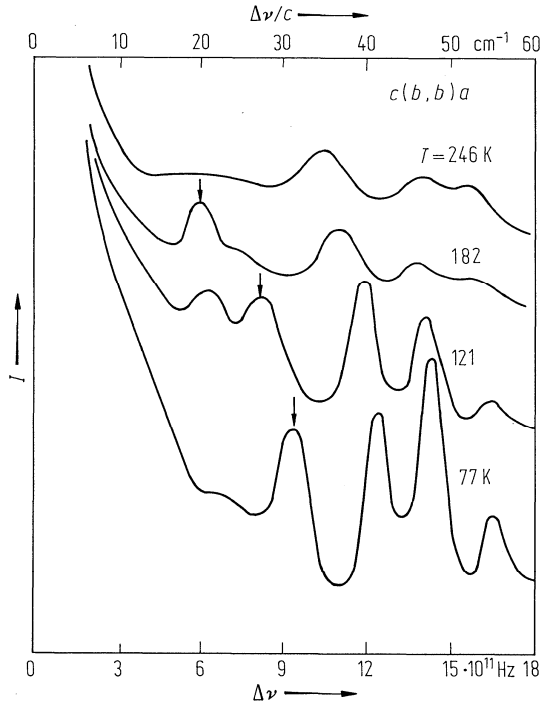

Fig. 39A-11-025. $(NH_4)_2ZnCl_4$. I vs. $\Delta\nu$ [81Smo]. Parameter: T. I: Raman scattering intensity. $\Delta\nu$: Raman shift.

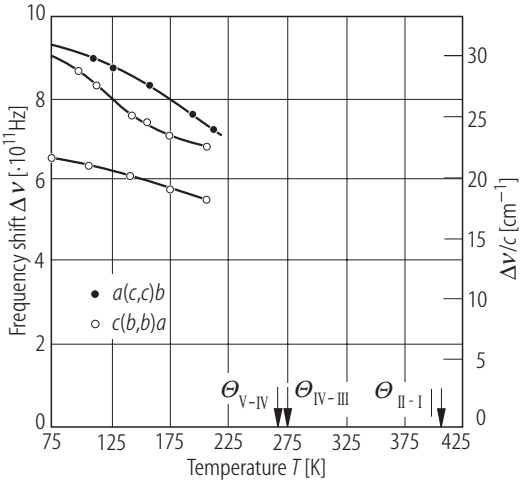

Fig. 39A-11-026. $(NH_4)_2ZnCl_4$. $\Delta\nu$ vs. T [81Smo]. $\Delta\nu$: Raman scattering frequency shift of low frequency modes.

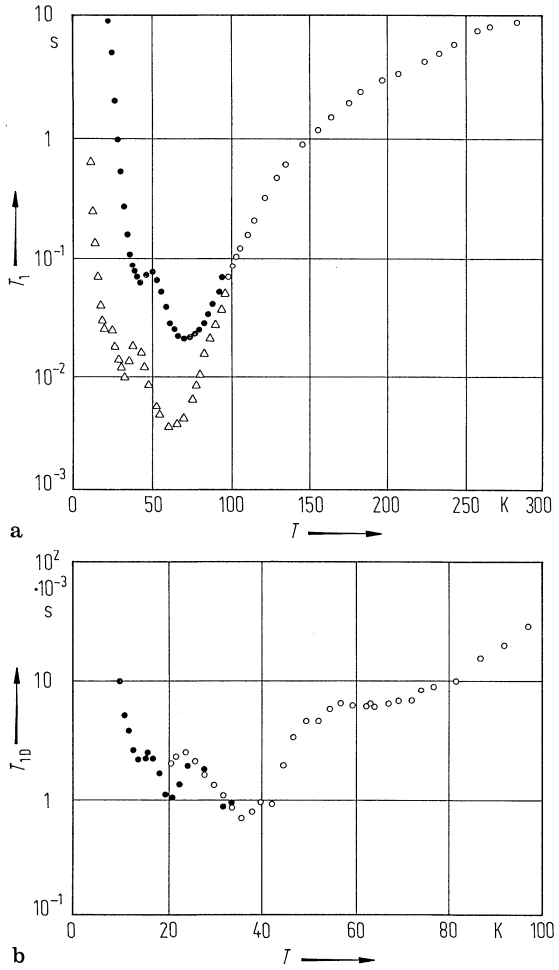

Fig. 39A-11-027. $(NH_4)_2ZnCl_4$. T_1, T_{1D} vs. T [85Ing]. T_1: proton spin-lattice relaxation time. T_{1D}: proton spin-lattice relaxation time in dipolar field. (**a**) ν_L = 6.3 MHz (open triangle), 18.5 MHz (open circle), 40 MHz (full circle). (**b**) ν_L = 12.6 MHz (open circle), 37 MHz (full circle).

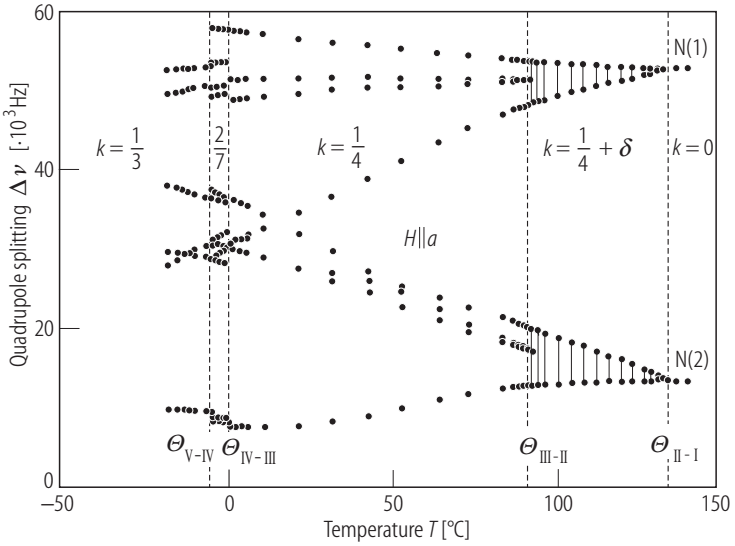

Fig. 39A-11-028. $(NH_4)_2ZnCl_4$. $\Delta\nu$ vs. T [91Mic]. $\Delta\nu$: first order quadrupole splitting in the ^{14}N NMR spectra. In the commensurate phases and the incommensurate phase the frequencies are given for discrete lines and edge singularities, respectively. k: modulation wavenumber in unit of c^*, and c^* represents the reciprocal lattice constant in phase I.

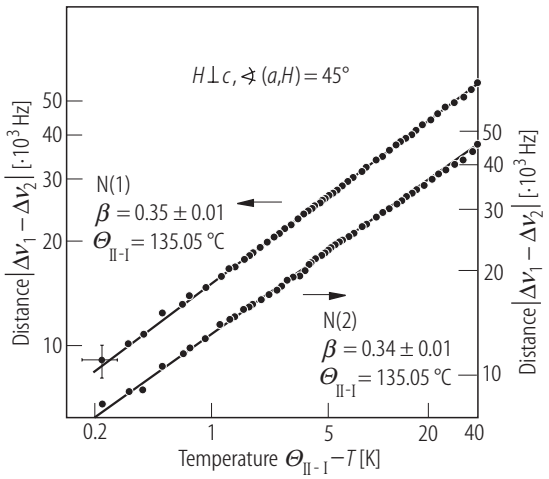

Fig. 39A-11-029. $(NH_4)_2ZnCl_4$. log-log plot of $|\Delta\nu_1 - \Delta\nu_2|$ vs. $\Theta_{II-I} - T$ in phase II [91Mic]. $|\Delta\nu_1 - \Delta\nu_2|$: distance of the edge singularities in the ^{14}N NMR spectra. β: critical exponent of width, $|\Delta\nu_1 - \Delta\nu_2|$; $|\Delta\nu_1 - \Delta\nu_2| \propto (\Theta_{II-I} - T)^{\beta}$.

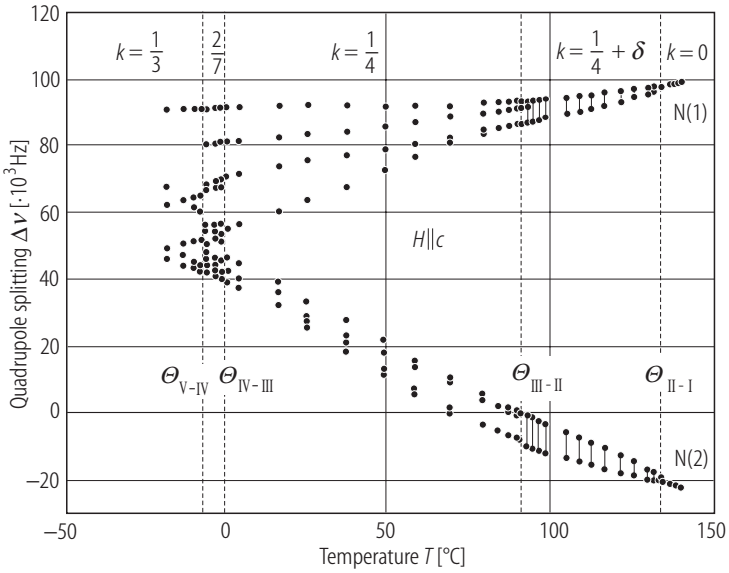

Fig. 39A-11-030. $(NH_4)_2ZnCl_4$. $\Delta\nu$ vs. T [91Mic]. $\Delta\nu$: first order quadrupole splitting. In the commensurate phases and the incommensurate phase the frequencies are given for discrete lines and edge singularities, respectively. k: modulation wavenumber in unit of c^*, and c^* represents the reciprocal lattice constant in phase I.

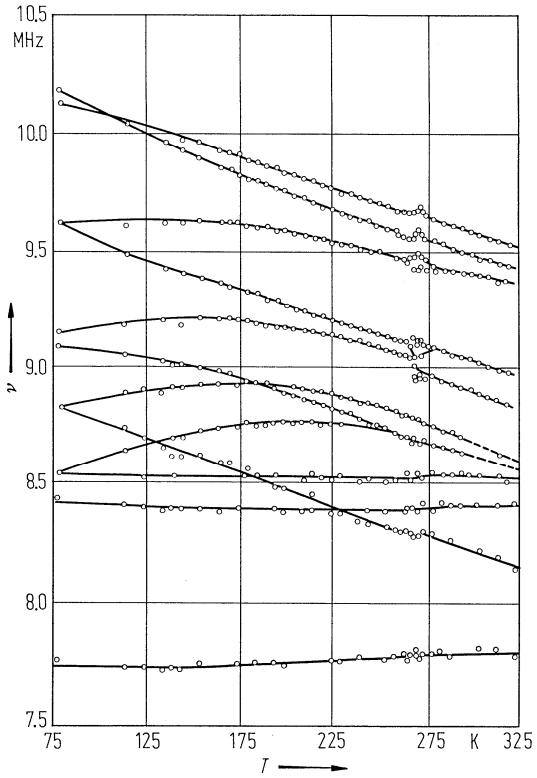

Fig. 39A-11-031. $(NH_4)_2ZnCl_4$. ν vs. T [80Ale]. ν: ^{35}Cl NQR frequency.

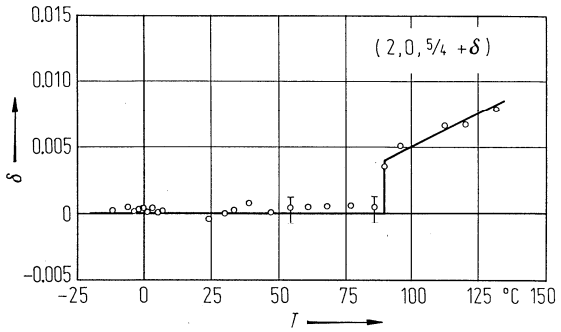

Fig. 39A-11-032. $(NH_4)_2ZnCl_4$. δ vs. T [84Sat]. δ is obtained from X-ray satellite reflection of (2, 0, 5/4 + δ).

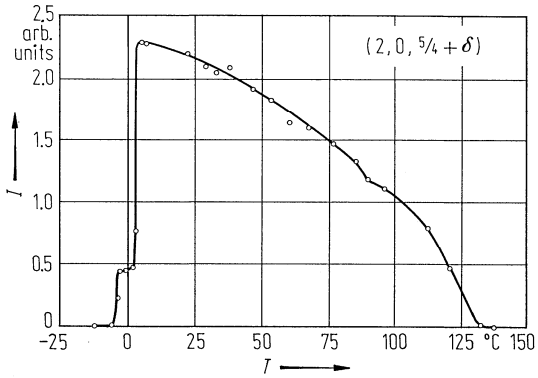

Fig. 39A-11-033. $(NH_4)_2ZnCl_4$. I vs. T [84Sat]. I: integrated intensity of X-ray reflection at (2, 0, 5/4 + δ).

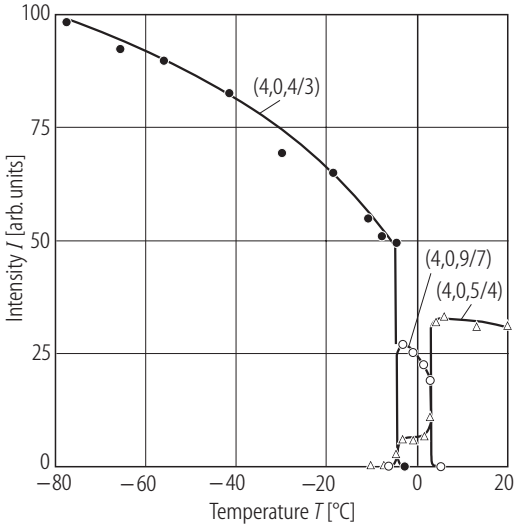

Fig. 39A-11-034. $(NH_4)_2ZnCl_4$. I vs. T [84Sat]. I: integrated intensities of X-ray reflections at (2, 0, 4/3), (4, 0, 9/7) and (4, 0, 5/4).